CHEMISTRY
A EUROPEAN JOURNAL

Organic–Inorganic Hybrids Based on Novel Bimolecular $[Si_2W_{22}Cu_2O_{78}(H_2O)]^{12-}$ Polyoxometalates and the Polynuclear Complex Cations $[Cu(ac)(phen)(H_2O)]_n^{n+}$ ($n=2$, 3)

Santiago Reinoso, Pablo Vitoria, Leire San Felices, Luis Lezama,* and Juan M. Gutiérrez-Zorrilla*[a]

Abstract: The reaction of a monosubstituted Keggin polyoxometalate (POM) generated in situ with copper–phenanthroline complexes in excess ammonium or rubidium acetate led to the formation of the hybrid metal organic–inorganic compounds $A_7[Cu_2(ac)_2(phen)_2(H_2O)_2][Cu_3(ac)_3(phen)_3(H_2O)_3][Si_2W_{22}Cu_2O_{78}(H_2O)]\cdot\approx 18\,H_2O$ (A = NH_4^+ (**1**), Rb^+ (**2**); ac = acetate; phen = 1,10-phenanthroline). These compounds are constructed from inorganic and metalorganic interpenetrated sublattices containing the novel bimolecular Keggin POM, $[Si_2W_{22}Cu_2O_{78}(H_2O)]^{12-}$, and Cu-ac-phen complexes, $[Cu(ac)(phen)(H_2O)]_n^{n+}$ ($n=2$, 3). The packing of compound **1** can be viewed as a stacking of open-framework layers parallel to the *xy* plane built of hydrogen-bonded POMs, and zigzag columns of π-stacked Cu-ac-phen complex cations running along the $[11\bar{1}]$ direction. Magnetic and EPR results are discussed with respect to the crystal structure of the compounds. DFT calculations on $[Cu(ac)(phen)(H_2O)]_n^{n+}$ cationic complexes have been performed, to check the influence of packing in the complex geometry and determine the magnetic exchange pathways.

Keywords: copper complexes · density functional calculations · magnetic properties · polyoxometalates

Introduction

Hybrid organic–inorganic materials have attracted an increasing interest in recent years owing to the possibility of combining the different characteristics of the components to get unusual structures, properties, or applications. Polyoxometalates (POM)[1] are one of the most widely used inorganic components in a wide range of fields, such as catalysis, medicine, molecular magnetism or material science,[2] owing to their extreme variability of composition, structure, electronic properties and applications. In this way, the design of new composite materials incorporating POMs and transition-metal (TM)-complex moieties constitutes an emerging area of interest. To date, several hybrid compounds based on vanadium[3] and molybdenum[4] isopolyanions have been reported, but in contrast, examples of Keggin heteropolyanions and their derivatives as the inorganic component are still limited.[5]

Currently, we are exploring the applicability of TM-monosubstituted Keggin POMs and TM carboxylate dinuclear complexes for the preparation of new magnetically attractive hybrid compounds by auto-assembly processes of the inorganic and metalorganic building blocks generated in situ, as an alternative synthetic method to the hydrothermal techniques that are generally employed.[6] Our investigations on the Cu–ac–phen system (ac = acetate; phen = 1,10-phenanthroline) have shown that the reaction of Cu–phen complexes with the $[SiW_{11}O_{39}Cu(H_2O)]^{6-}$ Keggin POM and acetate anions in the presence of ammonium or rubidium cations leads not only to the formation of the expected $[Cu_2(ac)_2(phen)_2(H_2O)_2]^{2+}$ dimer and subsequent interaction with the POM, but also to further coordination of a Cu–ac–phen monomer to the mentioned dimer and to the condensation of the Keggin units. Herein, we report the synthesis, crystal structure, and magnetic properties of the isostructural hybrid compounds $A_7[Cu_2(ac)_2(phen)_2(H_2O)_2][Cu_3(ac)_3$-

[a] S. Reinoso, P. Vitoria, L. San Felices, Dr. L. Lezama, Prof. J. M. Gutiérrez-Zorrilla
Departamento de Química Inorgánica
Facultad de Ciencia y Tecnología, Universidad del País Vasco
PO Box 644, 48080 Bilbao (Spain)
Fax: (+34) 946-013-500
E-mail: qipledil@lg.ehu.es
qipguloj@lg.ehu.es

Supporting information for this article is available on the WWW under http://www.chemeurj.org/ or from the author.

DOI: 10.1002/chem.200400762

$(phen)_3(H_2O)_3][Si_2W_{22}Cu_2O_{78}(H_2O)]\cdot\approx 18H_2O$ ($A=NH_4^+$ (**1**), Rb^+ (**2**)), which are constructed from interpenetrated inorganic and metalorganic sublattices containing the novel bimolecular Keggin POMs, $[Si_2W_{22}Cu_2O_{78}(H_2O)]^{12-}$ and Cu–ac–phen trimers, $[Cu_3(ac)_3(phen)_3(H_2O)_3]^{3+}$, respectively. DFT calculations of the polynuclear cationic copper complexes have been performed to check the influence of packing in the complex geometry and determine the magnetic exchange pathways.

Results and Discussion

Description of the crystal structure: Compound **1** crystallizes in the triclinic space group $P\bar{1}$ with one $[Si_2W_{22}Cu_2O_{78}(H_2O)]^{12-}$ dimeric polyanion, one $[Cu_2(ac)_2(phen)_2(H_2O)_2]^{2+}$ dimer, one $[Cu_3(ac)_3(phen)_3(H_2O)_3]^{3+}$ trimer, seven ammonium ions, and one water of hydration in the asymmetric unit. In the case of compound **2**, cell parameters obtained from low-quality crystals[7a] and powder samples[7b] confirm that the compounds are isostructural. Crystallographic data for compound **1** are given in Table 1.

Table 1. X-ray crystallographic data for compound **1**.

formula	$C_{70}H_{131}Cu_7N_{17}O_{112}Si_2W_{22}$
M_w [g]	7520.5
cystal system	triclinic
space group	$P\bar{1}1$
Z	2
T [K]	293
a [Å]	17.786(1)
b [Å]	18.075(1)
c [Å]	23.922(1)
α [°]	89.109(3)
β [°]	88.035(4)
γ [°]	86.756(4)
V [Å^3]	7672.9(7)
ρ_{calcd} [g cm^{-3}]	3.183(3)
μ [mm^{-1}]	17.614
diffractometer	Xcalibur
θ limits [°]	2.9–25
collected reflections	44914
unique reflections (R_{int})	26272 (0.055)
observed reflections [$I>2\sigma(I)$]	14386
refined parameters	1431
max. res. electron density [e Å^3]	2.968
$R(F)$[a] [$I>2\sigma(I)$]	0.0582
$wR(F^2)$[a] (all data)	0.1467

[a] $R(F)=\Sigma||F_o|-|F_c||/\Sigma|F_o|$, $wR(F^2)=\Sigma(F_o^2-F_c^2)^2/\Sigma[w(F_o^2)]^{1/2}$.

The $[Si_2W_{22}Cu_2O_{78}(H_2O)]^{12-}$ POM can be described as the product of the condensation of two α-$[SiW_{11}CuO_{39}(H_2O)]^{6-}$ Keggin units, each of which consists of a central SiO_4 tetrahedron surrounded in an ideal C_s symmetry by four, vertex-sharing M_3O_{13} trimers of edge-sharing MO_6 octahedra. One of the Keggin units shows a preference for the copper atom in the Cu1 octahedron (83%), whereas the copper atom in the other Keggin unit is disordered over eight positions, with the occupancy factors in the range from 4% for W14 to 19% for W22, being 18% for W13. Thus, the Keggin units are bound by a Cu-O-W bridge in which the Cu1–O1 and W13–O1 lengths differ significantly (2.12 and 1.79 Å, respectively), and the Cu1-O1-W13 angle is 158°. These structural parameters are very similar to those of the Cu-O-W bridge (Cu–O 2.25, W–O 1.75 Å, Cu-O-W angle 158°) present in the $[SiW_{11}CuO_{39}]_n^{6n-}$ chain of the previously described compound $K_5[Cu(ac)(pmdien)][SiW_{11}CuO_{39}]\cdot 12H_2O$ (pmdien = *N*,*N*,*N*′,*N*″,*N*″-pentamethyldiethylentriamine.[11b] In this compound there is no disorder in the position of the transition metal inside the POM.

The terminal water molecule coordinated to the Cu atom in one Keggin unit is thus replaced by a terminal O atom bonded to a W atom of the other unit. The subsequent formation of a Cu-O-W bridge connects the two polyanions which are rotated by 110° with respect to each other (Figure 1). Although this type of TM-O-W bridge has been observed in cyclic[8] and chainlike polymolecular Keggin POMs with TM = Mn^{II},[9] Co^{II},[10] or Cu^{II},[11] to our knowledge $[Si_2W_{22}Cu_2O_{78}(H_2O)]^{12-}$ is the first bimolecular TM-disubstituted Keggin POM with this type of bridge reported.

Table 2 displays ranges and mean values of M–O bond lengths for both α-Keggin subunits of compound **1** together with the optimized ones for the copper-monosubstituted α-Keggin and the $[\alpha\text{-}SiW_{12}O_{40}]^{4-}$ polyanions. Owing to the disorder of the Cu atom over the whole of subunit 2, it has only been possible to give Cu–O bond data only for subunit 1. As can be seen, the only substantial difference between both monosubstituted subunits is the wider range of variation of the W-bridging–O lengths in subunit 1, owing to the distortion induced by the presence of a localized copper atom.

The Jahn–Teller effect associated with octahedral copper(II) ions in the POMs induces an elongation of monosub-

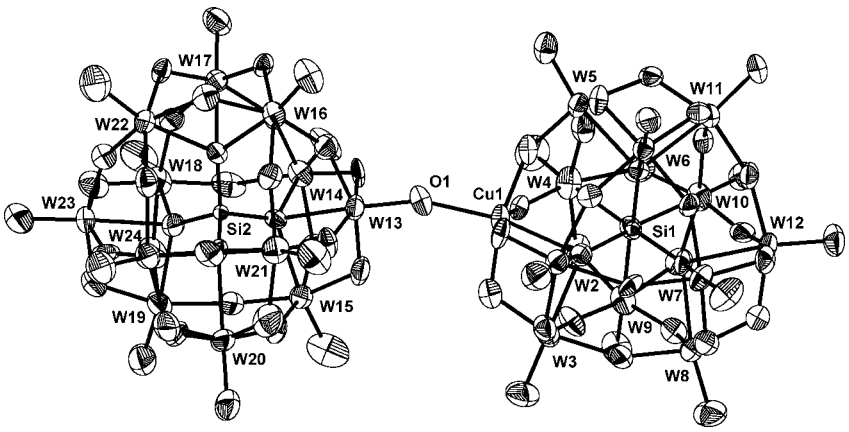

Figure 1. Structure of the bimolecular Keggin POM, $[Si_2W_{22}Cu_2O_{78}(H_2O)]^{12-}$ (ORTEP view).

Table 2. Ranges and (mean) M–O bond lengths [Å] for the POM in compound **1** and for the optimized polyanions.[a]

	Compound **1**: $[Si_2W_{22}Cu_2O_{78}(H_2O)]^{12-}$		Optimized polyanions	
	Subunit 1	Subunit 2	$[SiW_{11}O_{39}Cu(H_2O)]^{6-}$	$[SiW_{12}O_{40}]^{4-}$
W–O_a	2.28–2.39 (2.34)	2.30–2.37 (2.34)	2.32–2.44 (2.39)	2.393
W–O_b	1.78–2.02 (1.91)	1.85–1.98 (1.91)	1.81–2.03 (1.93)	1.923
W–O_c	1.79–2.06 (1.92)	1.88–1.96 (1.93)	1.82–2.03 (1.94)	1.935
W–O_t	1.70–1.76 (1.74)	1.69–1.83 (1.75)	1.76–1.77 (1.76)	1.740
Si–O_a	1.61–1.65 (1.63)	1.61–1.65 (1.63)	1.63–1.66 (1.65)	1.650
Cu–O_a	2.35		2.319	
Cu–O_b	1.96, 1.97		2.011	
Cu–O_c	1.98, 2.02		2.018	
Cu–O_t	2.12		2.286	
Cu–Si	3.446		3.377	
Si–$W_{Cu_{trans}}$	3.539		3.589	
W–Si	3.50–3.58 (3.53)	3.49–3.54 (3.52)	3.56–3.64 (3.60)	3.588
Cu–W_{trans}	6.983		6.964	
O_{Cu}–$O_{W_{trans}}$	10.781		10.709	
W–W_{trans}	7.01–7.09 (7.05)	7.02–7.07 (7.04)	7.15–7.21 (7.19)	7.172
O–O_{trans}	10.36–10.52 (10.44)	10.39–10.52 (10.46)	10.61–10.69 (10.66)	10.619

[a] O_a: oxygen atoms belonging to the central SiO_4 tetrahedron; O_b: bridging oxygen atoms between corner-sharing MO_6 octahedra; O_c: bridging oxygen atoms between edge-sharing MO_6 octahedra; O_t: terminal oxygen atoms.

stituted Keggin anions along the Cu–W_{trans} direction. Moreover, the different coordination sphere of Cu and W centers produces a distortion in the whole skeleton of the Keggin anion. This is nicely reproduced in the DFT-optimized structure and is also observed in the monosubstituted Keggin anion (see Figure S4 in the Supporting Information) present in the polymeric compound $K_5[Cu(ac)(pmdien)][SiW_{11}CuO_{39}]\cdot 12H_2O$.[11b] The longer equatorial Cu–O bond lengths (around 2 Å) promote a shortening of the corresponding W–O bonds (~1.80 Å) and a subsequent lengthening of equatorial W–O_{trans} ones (Figure 2). This effect propagates along the POM surface, attenuating towards the W atom opposite the Cu center, and leading to an alternating series of short and long W–O bonds. This fact is not observed either in copper-monosubstituted POM, where the copper atom is disordered over several positions (for example in subunit 2), or in the DFT-optimized nonsubstituted α-Keggin POM.

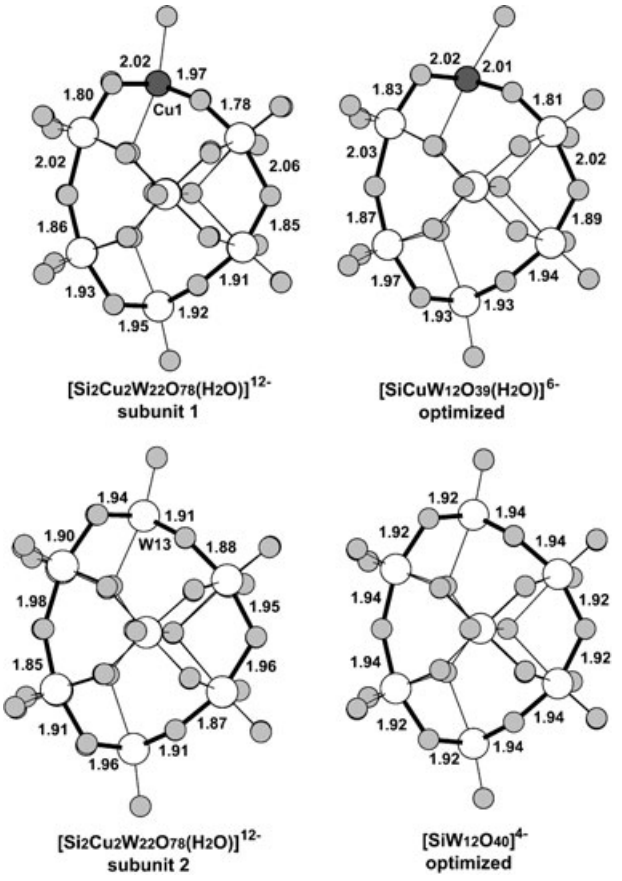

Figure 2. W–O equatorial bond length variations induced by the presence of a copper atom in monosubstituted Keggin POMs.

The $[Cu_2(ac)_2(phen)_2(H_2O)_2]^{2+}$ dimer is similar to that reported by Tokii and co-workers.[12] It comprises two square-pyramidal Cu atoms bridged by two acetate anions in a *syn–syn* fashion with a Cu–Cu length of 3.06 Å. Each basal plane is formed by two phenanthroline N atoms and two acetate O atoms, the apical position being occupied by a water molecule (Figure 3a). The phenanthroline ligands are almost parallel and ring-to-ring stacked, revealing intramolecular π interactions with average interplanar and intercentroidal distances of 3.46 and 3.61 Å, respectively.

The $[Cu_3(ac)_3(phen)_3(H_2O)_3]^{3+}$ trinuclear complex can be seen as the product of the axial coordination of a $[Cu(ac)(phen)(H_2O)_2]^+$ monomer (defined by the Cu6 coordination sphere) to a dimer (defined by Cu4 and Cu5) analogous to that described above. Thus, the apical water molecule of the square-pyramidal Cu5 atom is replaced by an acetate O atom (O108) belonging to the distorted 4 + 1 + 1 octahedral coordination sphere of Cu6. This fact results in the acetate anion acting as a μ_2-κ^1O,κ^2O bridge between the Cu atoms which are separated by 4.33 Å (Figure 3b). This type of bridging mode of the acetate ligand has been previously observed in $[Cu(ac)(dien)](ClO_4)$.[13] The geometric parameters of the Cu4–Cu5 fragment are similar to those of the dimer. On the other hand, the equatorial plane of Cu6 is composed of two phenanthroline N atoms, one acetate O atom, and one water molecule, the axial positions being occupied by one water molecule, and the O108 acetate oxygen atom. The phenanthroline ligands in the trimer are also almost parallel and ring-to-ring stacked: the geometry of the π interaction between phenanthrolines 4 and 5 is similar to that found in the dimer, whereas phenanthrolines 5 and 6 form an angle of 8°, and show similar interplanar and intercen-

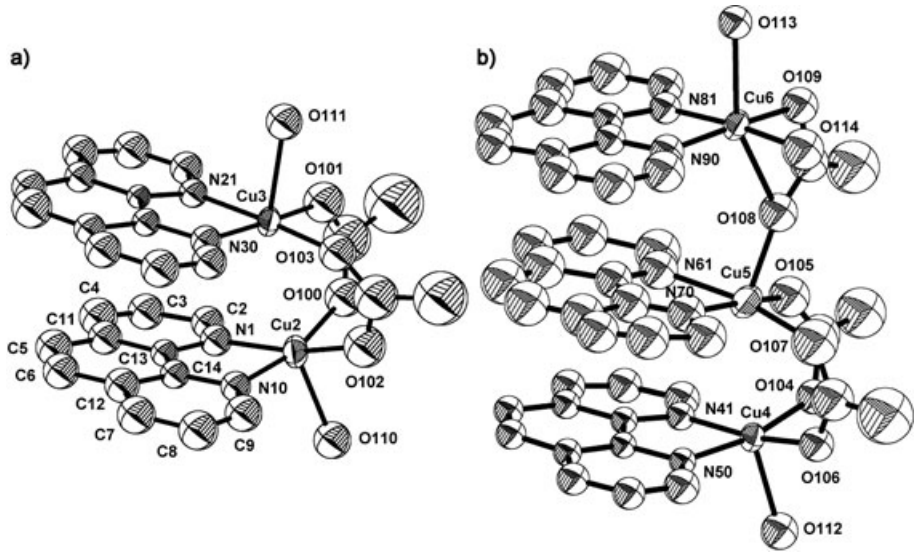

Figure 3. $[Cu(ac)(phen)(H_2O)]_n^{n+}$ cationic complexes: $n=2$ (a); $n=3$ (b) (ORTEP views).

troidal distances (3.55 and 3.58 Å, respectively). Selected bond lengths and angles for the cationic species are displayed in Table 3.

The inorganic sublattice consists of rows of $[Si_2W_{22}Cu_2O_{78}(H_2O)]^{12-}$ POMs running along the $[\bar{1}10]$ direction: the POMs are placed parallel to the *c* axis and hydrogen-bonded by ammonium ions, which alternatively interact with trimers and triads of two adjacent POMs (Figure 4a). These POM rows are further hydrogen bonded along the [110] direction by ammonium–water–ammonium links, which connect tetramers belonging to two neighboring

Table 3. Bond lengths [Å] and angles [°] for the experimental and optimized $[Cu(ac)(phen)(H_2O)]_n^{n+}$ cationic complexes.

	$[Cu_2(ac)_2(phen)_2(H_2O)_2]^{2+}$			$[Cu_3(ac)_3(phen)_3(H_2O)_3]^{3+}$		
	Compound **1**	B3LYP	Ref. 12		Compound **1**	B3LYP
Cu2 coordination sphere				Cu4 coordination sphere		
Cu2–O100	2.01(2)	1.931	1.939(6)	Cu4–O104	1.96(2)	1.946
Cu2–O102	1.93(2)	1.951	1.984(6)	Cu4–O106	1.94(2)	1.945
Cu2–N1	2.02(2)	2.008	2.010(7)	Cu4–N41	1.99(2)	2.027
Cu2–N10	2.02(2)	2.006	2.029(7)	Cu4–N50	2.00(2)	2.002
Cu2–0110	2.21(2)	2.290	2.201(7)	Cu4–O112	2.20(2)	2.297
O100-Cu2-O102	89.6(8)	92.7	92.8(2)	O104-Cu4-O106	89.9(6)	93.3
O100-Cu2-N10	165.9(8)	167.2	165.8(3)	O104-Cu4-N50	168.5(7)	174.0
O100-Cu2-O110	93.1(7)	97.5	92.2(2)	O104-Cu4-O112	90.8(6)	80.1
O102-Cu2-N1	167.1(8)	173.1	172.8(3)	O106-Cu4-ON41	168.9(7)	157.8
O102-Cu2-O110	92.4(7)	81.6	89.4(2)	O106-Cu4-O112	89.7(7)	102.9
N1-Cu2-N10	84.0(7)	83.0	81.6(3)	N41-Cu4-N50	82.9(6)	82.3
N1-Cu2-O110	100.4(7)	94.2	95.8(3)	N41-Cu4-O112	101.1(6)	99.3
N10-Cu2-O110	100.7(6)	94.8	100.9(3)	N50-Cu4-O112	100.5(6)	101.6
Cu3 coordination sphere				Cu5 coordination sphere		
Cu3–O101	1.96(2)			Cu5–O105	1.87(2)	1.963
Cu3–O103	1.93(2)			Cu5–O107	1.92(2)	1.963
Cu3–N21	2.01(2)			Cu5–N61	2.15(2)	2.023
Cu3–N30	1.97(2)			Cu5–N70	2.06(2)	2.022
Cu3–O111	2.28(2)			Cu5–O108	2.11(2)	2.337
O101-Cu3-O103	93.4(7)			O105-Cu5-O107	95.0(9)	94.20
O101-Cu3-N30	173.8(8)			O105-Cu5-N70	169.8(9)	169.6
O101-Cu3-O111	89.6(7)			O105-Cu5-O108	93.6(8)	97.2
O103-Cu3-N21	176.1(7)			O107-Cu5-ON61	168.1(9)	167.3
O103-Cu3-O111	90.8(6)			O107-Cu5-O108	91.0(9)	85.4
N21-Cu3-N30	84.1(7)			N61-Cu5-N70	78.4(9)	82.0
N21-Cu3-O111	91.0(6)			N61-Cu5-O108	96.5(8)	105.9
N30-Cu3-O111	92.4(6)			N70-Cu5-O108	93.8(8)	91.6
				Cu6 coordination sphere		
				Cu6–O109	2.00(2)	1.935
				Cu6–O114	1.97(2)	2.007
				Cu6–N81	1.96(2)	1.999
				Cu6–N90	2.00(2)	2.005
				Cu6–O113	2.33(2)	2.330
				Cu6–O108	2.56(2)	
				O109-Cu6-O114	92.2(7)	91.2
				O109-Cu6-N90	172.3(7)	163.4
				O109-Cu6-O113	94.0(6)	95.7
				O109-Cu6-O108	59.6(6)	
				O114-Cu6-N81	174.3(8)	170.8

Table 3. (Continued)

	$[Cu_2(ac)_2(phen)_2(H_2O)_2]^{2+}$ Compound **1**	B3LYP	Ref. 12		$[Cu_3(ac)_3(phen)_3(H_2O)_3]^{3+}$ Compound **1**	B3LYP
				O114-Cu6-O113	91.0(7)	81.2
				O114-Cu6-O108	87.2(7)	
				N81-Cu6-N90	82.2(8)	82.8
				N81-Cu6-O113	92.3(8)	107.3
				N81-Cu6-O108	91.9(7)	
				N90-Cu6-O113	91.6(7)	100.7
				N90-Cu6-O108	114.9(7)	
				O113-Cu6-O108	153.5(6)	
Cu2···Cu3	3.056(4)	3.300	3.063(3)	Cu4···Cu5	3.087(4)	3.952
				Cu5···Cu6	4.331(4)	5.536
basal and aromatic ligand plane dihedral angles[a]						
Cu2–phen2	20.7(6)	6.7	9.9	Cu4–phen4	14.3(6)	10.1
Cu3–phen3	2.0(6)			Cu5–phen5	10.0(8)	5.3
				Cu6–phen6	1.1(7)	5.7
Cu2–Cu3	22.5(7)	41.6	22.9	Cu4–Cu5	24.0(8)	73.1
				Cu5–Cu6	16.5(8)	79.1
phen2–phen3	3.9(5)	44.4	4.9	phen4–phen5	1.1(6)	65.6
rotation angle[b]	3.7(6)	25.2	4.9	rotation angle	12.3(7)	
				phen5–phen6	7.6(6)	79.5
				rotation angle	−10.4(7)	

[a] Planes: Cu2: O100, O102, N1, N10; Cu3: O101, O103, N21, N30; Cu4: N41, N50, O104, O106; Cu5: N61, N70, O105, O107; Cu6: N81, N90, O109, O114; phen2: N1, N10, C2–C14; phen3: N21, N30, C22–C34; phen4: N41, N50, C42–C54; phen5: N61, N70, C62–C74; phen6: N81, N90, C82–C94. [b] The rotation angle between phenanthrolines i and j is defined by the average value of the following C_i-Cu_i-Cu_j-C_j torsion angles: i = 2, j = 3: C13-Cu2-Cu3-C33, C14-Cu2-Cu3-C34; i = 4, j = 5: C53-Cu4-Cu5-C73, C54-Cu4-Cu5-C74; i = 5, j = 6: C73-Cu5-Cu6-C93, C74-Cu5-Cu6-C94.

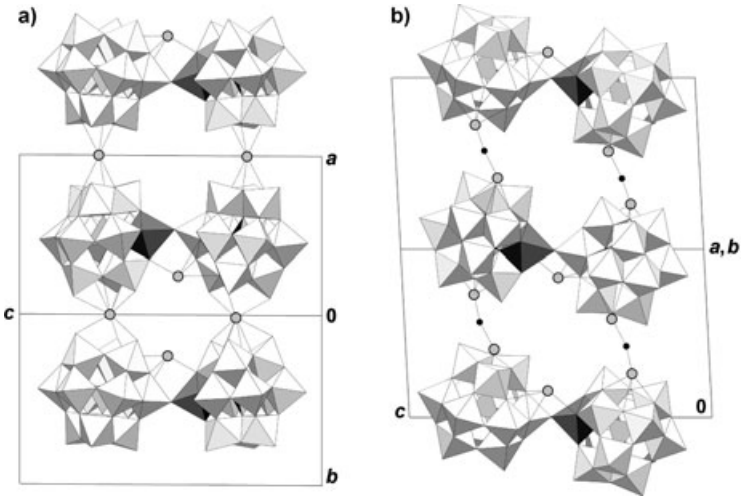

Figure 4. Views of the inorganic sublattice along a) the [110] and b) the [$\bar{1}$10] directions. Copper centers are represented as dark octahedra, ammonium cations as large gray circles, and water molecules as small black circles.

POMs of adjacent rows (Figure 4b). This type of arrangement leads to open-framework inorganic layers parallel to the (001) plane.

The $[Cu_2(ac)_2(phen)_2(H_2O)_2]^{2+}$ dimers (d) are embedded in POM layers with their O and C atoms involved in a extended network of N–H···O and C–H···O interactions with the ammonium ions and the POM surface, respectively. On the other hand, the $[Cu_3(ac)_3(phen)_3(H_2O)_3]^{3+}$ trimers (t) occupy the interlaminar space between adjacent layers in such a way that zigzag metalorganic columns are formed

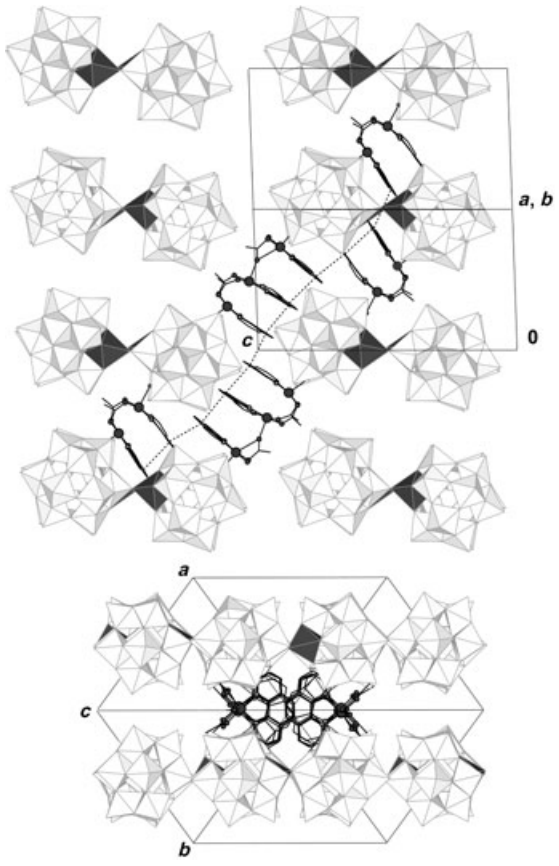

Figure 5. View of a metalorganic column crossing the inorganic sublattice: (top) in the ($\bar{1}$10) plane, dotted lines indicate intermolecular π interactions; (bottom) along the [11$\bar{1}$] direction. Ammonium cations and water molecules have been removed for clarity.

that cross the inorganic framework obliquely in the [11$\bar{1}$] direction (Figure 5).

The metalorganic columns show a dimer-trimer-trimer-dimer (..d-t-t-d..) sequence, with the cationic species held together by π interactions involving the central ring of the phenanthroline ligands. The most favorable π interaction occurs between the trimers. In contrast, those involving the dimers are less favorable owing to the geometric constraints imposed by the inorganic sublattice. Thus, in the case of the interaction between dimers and trimers, a lengthening of the average interplanar and intercentroidal distances owing to the tilting of the ligands (12°) is observed. Moreover, the dimer–dimer interaction, which takes place in the space between two adjacent POMs in a row, shows a long intercentroidal distance (4.27 Å) between the parallel ligands placed at an interplanar distance of 3.44 Å. This results in a small overlap of the aromatic rings. Intramolecular and intermolecular contacts for the cationic species are listed in Table 4.

Table 4. Inter and intramolecular π interactions for the cationic complexes in compound **1**.[a]

		DZ [Å]	ANG [°]	DC [Å]
intermolecular π interactions				
dimer–trimer	Cg2–Cg6^{i}	3.21(2)	12.2(8)	3.65(2)
trimer–trimer	Cg4–Cg4^{ii}	3.29(1)	0.0(6)	3.53(1)
trimer–dimer	Cg6–Cg2^{i}	3.50(2)	12.2(8)	3.65(2)
dimer–dimer	Cg3–Cg3^{i}	3.44(1)	0.0(6)	4.27(1)
intramolecular π interactions				
dimer	Cg2–Cg3	3.46(1)	4.3(7)	3.61(1)
trimer	Cg4–Cg5	3.42(2)	1.1(8)	3.56(2)
trimer	Cg5–Cg6	3.55(2)	8.2(8)	3.58(2)

[a] Cgi: centroid of the central ring of phenanthroline i (i=2: C5, C6, C11–C14; i=3: C25, C26, C31–C34; i=4: C45, C46, C51–C54; i=5: C65, C66, C71–C74; i=6: C85, C86, C91–C94); DZ: perpendicular distance of Cgi on ring j; ANG: dihedral angle between planes i and j; DC: distance between ring centroids. Symmetry codes: i: $1-x$, $1-y$, $1-z$; ii: $2-x$, $2-y$, $-z$.

Optimizations of both copper cationic complexes have been performed to examine the influence of the packing on their geometries. Whereas the calculated bond lengths and angles show a good agreement with experimental data (Table 3), there are noticeable differences in the basal and aromatic ligand plane dihedral angles. Although in the experimental compounds the phenanthroline ligands are almost parallel and ring-to-ring stacked with dihedral angles smaller than 8°, the optimized cationic complexes show a much more open and twisted structure. Thus, in the dimeric fragments the angles are 44.4° and 65.6° for the dimer and trimer, respectively. The most remarkable fact is that phen5 and phen6 ligands are almost perpendicular. These observations confirm the importance of π interactions not only in the crystal packing of compounds containing aromatic rings, but also in determining the geometry of these rather floppy complexes.

EPR spectroscopy: X-band powder EPR spectra of compound **1** recorded at different temperatures between 4.2 and 290 K are illustrated in Figure 6 (similar results obtained for compound **2** are included in the Supporting Information). The room-temperature X-band spectrum displays a broad anisotropic resonance centered at approximately 3200 G, as expected for copper(II) systems. Moreover, three less intense signals are observed at about 1600, 2500, and 3900 G. Such spectra are usually associated with well-isolated triplet spin states with relatively small zero-field splitting. The low-field signal corresponds to a $\Delta M_S = \pm 2$ forbidden transition. Lowering the temperature of the samples to 4.2 K results in better resolution of the central (3200 G) line, with partially resolved hyperfine structure. On the other hand, the intensity of the other resonances diminishes with temperature below 100 K, and the signals vanish at 4.2 K, in line with strong antiferromagnetic coupling.

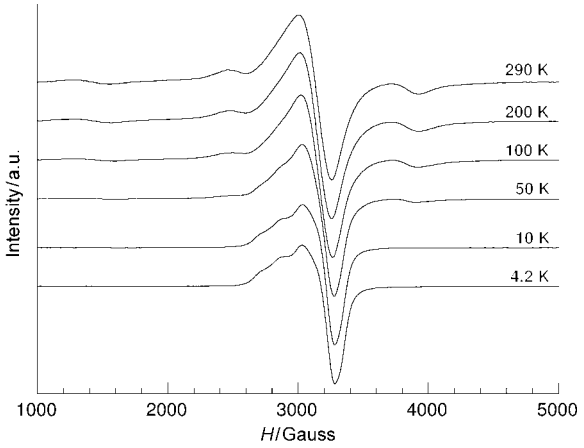

Figure 6. Temperature dependence from 4.2 to 290 K of the powder X-band EPR spectra for compound **1**.

The severe overlap of the individual lines in the $\Delta M_S = \pm 1$ region precludes any attempt to extract the principal components of the g tensors or to evaluate the zero-field splitting from the X-band spectra. Q-band EPR experiments were therefore performed between 120 and 290 K, which led to a considerable improvement of the resolution of the spectra (Figure 7). In addition to the half-field signal (ca. 5700 G), at least eight more signals can be detected between 9500 and 12500 G.

In spite of the presence of seven different copper(II) chromophores in both compounds, the number of observable EPR signals must be drastically reduced by the averaging effects of the magnetic exchange. In fact, taking into account the structural features and possible exchange pathways, a maximum of three contributions to the EPR spectra could be expected. The simplest one is that corresponding to the copper in monosubstituted POMs. As previously analyzed in analogous systems,[6] this paramagnetic center gives rise to an axial EPR signal ($g_{\parallel} = 2.426$; $g_{\perp} = 2.095$) with well-defined hyperfine structure in the parallel region of the spec-

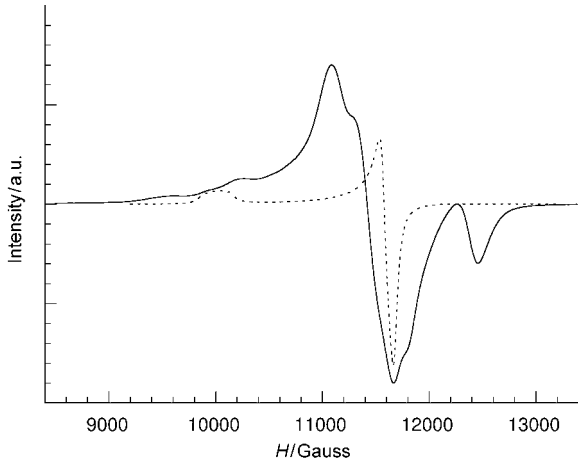

Figure 7. Q-band EPR powder spectrum for compound **1** registered at 120 K. The dotted line shows the expected contribution of the copper substituted POMs.

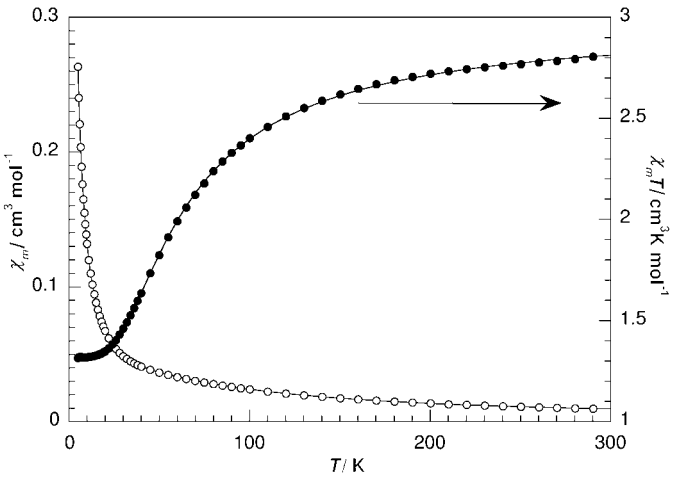

Figure 8. Thermal evolution of the magnetic susceptibility and $\chi_m T$ product for compound **1**. Continuous lines represent the least-squares fit to Equation (1).

trum ($A_{\parallel} = 90 \times 10^{-4}\,cm^{-1}$). Another set of EPR lines must come from the $[Cu_2(ac)_2(phen)_2(H_2O)_2]^{2+}$ dimers. Owing to the nonfavorable π stacking of the phenanthroline rings, these entities are probably isolated from a magnetic point of view, giving rise to typical triplet state EPR spectra. Finally, the contribution of the $[Cu_3(ac)_3(phen)_3(H_2O)_3]^{3+}$ trinuclear species is more difficult to predict, but the higher nuclearity and the favorable intertrimeric π interactions probably lead to a broad unresolved band in the $g=2$ region.

According to the analysis above, two of the resonances observed in the Q-band spectra (see Figure 7), as well as the low-temperature X-band signal, can be attributed to the monomeric species. On the other hand, no evidence of signals corresponding to isolated trimeric entities has been found. The rest of the observed resonances are consistent with a triplet spin state and must be ascribed to the $[Cu_2(ac)_2(phen)_2(H_2O)_2]^{2+}$ dimers. We have tried to fit them using the reported formulae for the transition fields along the principal axes,[14] but no reasonable fitting was obtained, suggesting the existence of noncollinear g and D tensors. This misalignment between g and D is not surprising taking into account the fact that the orthogonal axes to the equatorial planes of the copper chromophores present an appreciable deviation with respect to the copper–copper intradimer direction.[15]

Magnetic properties: The thermal evolution of the magnetic molar susceptibility and the $\chi_m T$ product, being $\chi_m T = \mu_{eff}^2/8$, is displayed in Figure 8 for compound **1** and in the Supporting Information for compound **2**. For both compounds, χ_m increases continuously with decreasing temperature and no maximum is observed. At high temperature ($T > 150$ K), the susceptibility data are well described by Curie–Weiss expressions, being $C_m = 3.04\,cm^3\,K\,mol^{-1}$, $\theta = -24.1$ K for **1** and $C_m = 3.06\,cm^3\,K\,mol^{-1}$, $\theta = -21.8$ K for **2**. The values of $\chi_m T$ at 300 K for compounds **1** and **2** are 2.827 and 2.867 $cm^3\,K\,mol^{-1}$, respectively, which are in good agreement with the presence of seven noncorrelated Cu^{II} ions (2.625 $cm^3\,K\,mol^{-1}$, considering $g=2$). Additionally, when the systems are cooled down from 300 to approximately 20 K, the $\chi_m T$ product decreases reaching values close to 1.32 $cm^3\,K\,mol^{-1}$, and remains approximately constant below 20 K. This behavior indicates the presence of relatively strong antiferromagnetic interactions between some of the Cu^{II} ions, whereas the rest appear to be uncoupled.

The simultaneous presence of trimeric, dimeric, and monomeric Cu^{II} entities in these compounds, together with the absence of significant peaks in the susceptibility curves, makes an exact theoretical treatment of the experimental data practically impossible. To obtain an operative expression for the magnetic susceptibility that allows us to evaluate the strength of the different exchange interactions, some approximations are needed to reduce the large number of adjustable parameters. In this way, we have compared the experimental curves with those calculated with Equation (1), where N, β, and k have their usual meaning, g is the average g-factor of the copper–acetate–phenanthroline complexes and g' is the local g-factor of the Cu-monosubstituted Keggin-POMs.

$$\chi_m = \frac{Ng^2\beta^2[1+\exp(-\Delta_1/kT)+10\exp(-\Delta_2/kT)]}{4kT[1+\exp(-\Delta_1/kT)+2\exp(-\Delta_2/kT)]} + \frac{2Ng^2\beta^2}{kT[3+\exp(-J_D/kT)]} + \frac{2Ng'^2\beta^2}{4kT} \quad (1)$$

The first term in Equation (1) corresponds to the magnetic molar susceptibility of a $S = {}^1/_2$ linear trimer with a negligible interaction between nonadjacent ions.[16] Δ_1 and Δ_2 are the energy gaps between the three spin states of the trimer, being related to the exchange parameters (J_{T1} for Cu4–Cu5 and J_{T2} for Cu5–Cu6) through Equations (2)–(5).

$$\Delta_1 = E(1/2,-) - E(1/2,+) \quad (2)$$

$$\Delta_2 = E(3/2) - E(1/2,+) \quad (3)$$

$$E(3/2) = -(J_{T1} + J_{T2})/4 \quad (4)$$

$$E(1/2,\pm) = (J_{T1} + J_{T2})/4 \pm \sqrt{[(J_{T1} - J_{T2})^2 + J_{T1}{}^2 + J_{T2}{}^2]/8} \quad (5)$$

The second term in Equation (1) is the classical Bleaney–Bowers equation for a dinuclear copper(II) complex,[17] being J_D, the singlet–triplet energy gap; and the last term corresponds to the paramagnetic contribution of the copper substituted POMs. Intermolecular interactions have been intentionally suppressed to avoid an excessive number of variables.

Least-square fits of Equation (1) to the data were performed by minimizing the function (6), where NP is the number of data points and NV is the number of variable parameters.

$$R = \{ \sum_{i=1}^{NP} [\chi_m(\exp)_i - \chi_m(\mathrm{cal})_i]^2 / (NP - NV) \}^{1/2} \quad (6)$$

If all five magnetic parameters are allowed to vary freely in the fitting procedure, many sets of solutions are obtained depending on the starting points. Therefore, we tried to introduce some restrictions. First, the g' value was held fixed at 2.204, as deduced from the EPR spectra, and the number of possible solutions decreases considerably. Second, as can be seen in DFT-calculated frontier molecular orbitals for the trimer (Figure 9b), the Cu5–Cu6 exchange pathway involves the nonmagnetic d_{z^2} orbitals of the Cu^{II} ions and it is significantly longer than the Cu4–Cu5 one. J_{T2} was therefore allowed to vary only between $-J_{T1}/10$ and $J_{T1}/10$. Within these hypotheses, two reasonable solutions were obtained (Table 5) that showed a very good agreement between experimental and fitted data (Figure 8).

Table 5. Least-squares-fitted experimental and DFT calculated coupling constants (cm^{-1}) for the $[Cu(ac)(phen)(H_2O)]_n^{n+}$ cationic complexes.

		Trimer		Dimer	
Compound/fit	g	J_{T1}	J_{T2}	J_D	R (x10^4)
1/[A]	2.11	−80.7	−0.04	−80.7	2.88
1/[B]	2.11	−74.1	3.90[a]	−89.5	2.87
2/[A]	2.13	−81.3	−0.23	−81.3	8.91
2/[B]	2.13	−70.6	3.42[a]	−96.8	8.71
basis set					
6–31G(d)		−65.5	0.46	−77.0	
TZVP+DZ		−92.7	0.43	−116.8	
TZVP+SVP		−70.3	0.50	−88.7 (−89)[b]	
TZVP+SVP+SV		−70.7	0.50	−89.5	

[a] The J_{T2} coupling constant value is poorly defined and severely overestimated by the fitting procedure. Such a high value would be noticeable in the χ_m and $\chi_m T$ curves, and it can be safely assumed that its real value is much closer to zero. [b] Value obtained from ref. [19] calculated using B3LYP and a very similar basis set to the one used in this work.

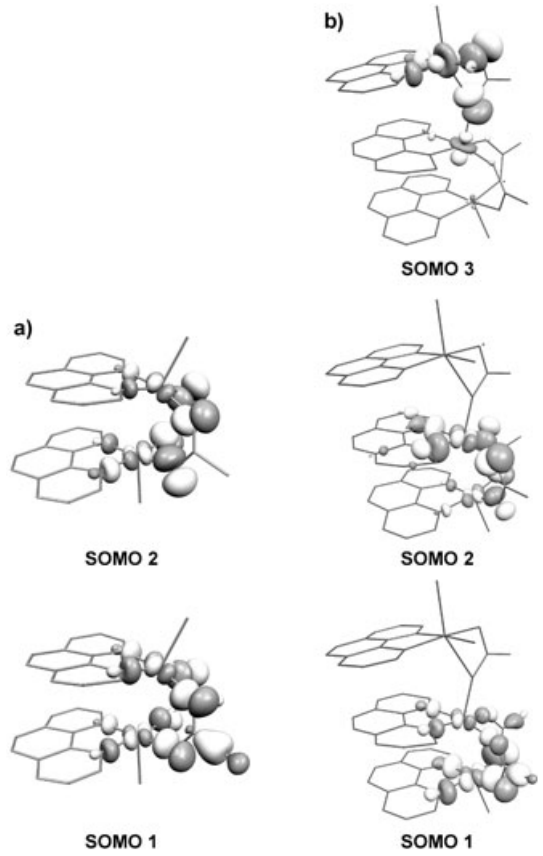

Figure 9. DFT-calculated frontier single-occupied molecular orbitals (SOMOs) for $[Cu(ac)(phen)(H_2O)]_n^{n+}$ cationic complexes: $n=2$ (a); $n=3$ (b).

Starting the fitting process with identical J_{T1} and J_D values, solution A was obtained. The corresponding set of calculated parameters implies that magnetic interactions between the Cu4 and Cu5 atoms of the trimeric entities and the Cu2 and Cu3 atoms of the dimers are of similar strength, in good agreement with the close geometry of both fragments. Moreover, the low J_{T2} value obtained indicates negligible exchange through the *syn–anti* single acetate bridge of the trimer units. Therefore, for this solution the system could be considered as the sum of two independent dimers plus a monomeric contribution. This assumption is supported by the observed $\chi_m T$ values at low temperatures, which are in good agreement with those expected for three magnetically independent Cu^{II} ions. Moreover, the calculated J values are also in concordance with the deduced Weiss temperatures, which must be approximately one half of the exchange integrals for dimeric systems with $S = {}^1/_2$.[18]

A somewhat different solution B is obtained when nonequivalent exchange constants are utilized as starting parameters. In this case, the calculated intradimeric interactions are larger than the intratrimeric ones. It is noteworthy that the obtained singlet–triplet energy gap for the dimer ($\approx -89\ cm^{-1}$) agrees better than the one fitted by solution A with the experimental value of $-86\ cm^{-1}$ obtained by Tokii et al. for $[Cu(ac)(phen)(H_2O)]_2(NO_3)\cdot 4H_2O$. This complex

exhibits a similar dimeric unit with the calculated value ($-89\ cm^{-1}$) using the same procedure as the one used in this work.[19] Besides, even if this solution yields slightly lower R values, the calculated curves are similar. Thus, DFT calculations have been carried out for the experimental geometries to identify the most correct description of the system.

Regardless of the basis set used, all calculations afford magnetic coupling constants that qualitatively support the solutions given by fitting B. Antiferromagnetic interactions are larger in the dimer than in the trimer, the ratio J_D/J_{T1} in the range 1.2–1.3 is in good agreement with the fitted data and a very small ferromagnetic coupling between the dimeric fragment and the $[Cu(ac)(phen)(H_2O)_2]^+$ monomer of the trimer (Table 5). In fact, the calculated exchange parameters with the basis set of highest quality (triple-962 valence for the metal atoms and split valence for the rest, with polarization functions in all of them (TZVP+SVP)) deviates by less than 5% from the fitted experimental data afforded by fitting B.

The significant difference between the magnetic coupling constants of the dimer and the dimeric unit of the trimer could be due, in principle, to two main factors: 1) variations in the geometrical parameters, especially those related to the coordination sphere of copper atoms, and 2) changes in one apical ligand, such as replacement of a water molecule in the dimer by the $[Cu(ac)(phen)(H_2O)_2]^+$ group bridged to the dimeric subunit through an acetate ligand. To check the influence of this second factor the exchange coupling constant has been calculated for the dimeric subunit of the trimer, without modifications in the geometry except that a water molecule replaced the $[Cu(ac)(phen)(H_2O)_2]^+$ group in the apical position. The result, $-69.1\ cm^{-1}$, is almost identical to the experimental and calculated values for the trimer, which indicates that this apical replacement has negligible influence on the value of the coupling constant. Thus, the difference must be attributed to a coupled and complex variation in several geometrical parameters between the dimer and the trimer.

Conclusion

The reaction between a copper monosubstituted Keggin POM and Cu–ac–phen complexes generated in situ affords a hybrid inorganic–metalorganic compound based on inorganic and metalorganic interpenetrated sublattices. The former consists of a bidimensional arrangement of the hydrogen-bonded bimolecular Keggin POM, $[Si_2W_{22}Cu_2O_{78}(H_2O)]^{12-}$, a product of the condensation of two α-$[SiW_{11}CuO_{39}(H_2O)]^{6-}$ Keggin units by formation of a Cu-O-W bridge. To our knowledge this is the first discrete bimolecular TM-disubstituted-Keggin POM reported. The metalorganic sublattice is formed by copper complexes of general formula $[Cu(ac)(phen)(H_2O)]_n^{n+}$ ($n=2$, 3), which π stack along the $[11\bar{1}]$ direction.

DFT calculations on $[Cu(ac)(phen)(H_2O)]_n^{n+}$ cationic complexes have shown the strong influence of packing on the complex geometry. In the crystal structure, the phenanthroline ligands are disposed almost parallel to each other to facilitate both intra- and intermolecular π interactions. In the calculated structures, the parallel arrangement is lost in favor of very open and twisted structures with angles between the phenantholine planes ranging from 45 to 80°.

EPR studies show a strong antiferromagnetic coupling between copper atoms in the $[Cu(ac)(phen)(H_2O)]_n^{n+}$ cationic complexes and the presence of magnetically isolated copper atoms in each Keggin subunit of the POM.

Magnetic susceptibility studies together with the invaluable help of DFT calculations of the magnetic coupling constants, confirm the presence of antiferromagnetic coupling in the dimer and the dimeric unit of the trimer. They also indicate negligible exchange through the *syn–anti* single acetate bridge of the trimer units. DFT calculations show that the significant difference between the magnetic coupling constants of the dimer and the dimeric unit of the trimer must be attributed to variations in several geometrical parameters between the dimer and the trimer, whereas the replacement of an apical water ligand by an acetate bridge has a negligible influence.

Experimental Section

All reagents were used as purchased without further purification. The $K_8[\alpha\text{-}SiW_{11}O_{39}]$ precursor was synthesized as described in reference [20]. Microanalyses: C, H, N: LECO CHNS-932 analyser; Cu, Rb: Perkin-Elmer 4110ZL analyser. FTIR: Mattson 1000 FT-IR spectrometer. TG/DTA: TA Instruments SDT2960 thermobalance (100 mL min^{-1} flow, synthetic air; 20–600 °C at a rate of 5 °C min^{-1}).

Synthesis of 1: A solution of $CuCl_2{\cdot}2H_2O$ (34 mg, 0.2 mmol), $K_8[\alpha\text{-}SiW_{11}O_{39}]$ (644 mg, 0.2 mmol), and an excess of ammonium acetate in water (30 mL) was heated to 100 °C for 1 h. A solution containing $CuCl_2{\cdot}2H_2O$ (68 mg, 0.4 mmol) and 1,10-phenanthroline (79 mg, 0.4 mmol) in water (30 mL) was added, and a blue precipitate appeared. The reaction mixture was stirred for 2 h, then the precipitate was removed by filtration. Prismatic blue crystals suitable for X-ray diffraction were obtained from the mother liquor by slow evaporation. Elemental analysis calcd (%) for $C_{70}Cu_7H_{95}N_{17}O_{94}Si_2W_{22}{\cdot}18H_2O$: C 11.14, H 1.75, N 3.15, Cu 5.89; found: C 10.89; H 1.65; N 3.20; Cu 5.74; IR (KBr pellets): acetate: $\tilde{\nu}=1622$ (w), 1578 (m), 1421 (m); POM: 1003 (w), 951 (s), 901 (vs), 795 (vs), 687 (s), 534 cm^{-1} (m); themogravimetric(TG)/differential thermogravimetric analysis (DTA) shows a dehydration step below 150 °C partially overlapped with the collapse of the crystal structure; it involves the loss of approximately 22 water molecules.

Synthesis of 2: Compound **2** was prepared by a method similar to that used for the synthesis of **1** except that an excess of rubidium acetate was employed. Elemental analysis calcd (%) for $C_{70}Cu_7H_{67}N_{10}O_{94}Rb_7Si_2W_{22}{\cdot}18H_2O$: C 10.48, H 1.29, N 1.75, Cu 5.55, Rb 7.46; found: C 10.54, H 1.21, N 1.72, Cu 5.40, Rb 7.66; IR (KBr pellets): acetate: $\tilde{\nu}=1624$ (w), 1577 (m), 1425 (m); POM: 1003 (w), 947 (s), 897 (vs), 793 (vs), 683 (s), 534 cm^{-1} (m); TG/DTA shows a dehydration step below 150 °C partially overlapped with the collapse of the crystal structure; it involves the loss of approximately 24 water molecules.

Magnetic measurements and EPR spectra: *Magnetic susceptibility*: Quantum Design MPMS-7 SQUID magnetometer (T range: 5–300 K; applied field: 0.1 T; diamagnetic corrections: estimated from Pascal's constants). *EPR powder spectra*: Bruker ESP300 spectrometer (X and Q bands) equipped with Oxford low temperature devices (magnetic field calibration: NMR probe; determination of the frequency inside the cavity:

Hewlett-Packard 5352B microwave frequency counter; maintenance of the crystal structures in powder samples was confirmed by powder X-ray diffraction; computer simulation: WINEPR-SimFonia, version 1.5, Bruker Analytische Messtechnik GmbH).

X-ray crystallography: Data collection for **1** and **2** was performed at room temperature on a Xcalibur single-crystal diffractometer (graphite monochromated MoK_α radiation, $\lambda = 0.71073$ Å), fitted with a Sapphire CCD detector. For compound **1**, a total of 1532 frames of data was collected with an exposure time of 20 s per frame, using the ω-scan technique with a frame width of $\Delta\omega = 0.30°$. Data frames were processed (unit cell determination, intensity data integration, correction for Lorentz and polarization effects, and analytical absorption correction) using the CrysAlis software package.[21] Neutral atom scattering factors and anomalous dispersion factors were taken from the literature.[22] The structure was solved by using direct methods (DIRDIF 99).[23] Heavy atoms and the oxygen atoms belonging to the polyanion were refined anisotropically by a full-matrix least-squares refinement of F^2. Copper atoms in the polyanion were delocalized over all tungsten positions and their population parameters were refined without restriction, resulting in the expected number of one copper ion per Keggin subunit. Hydrogen atoms of the phenanthroline and acetate species were placed in calculated positions and refined with a riding model. SHELXL97[24] was used for structure refinement of the compounds. The crystallographic calculations were performed by using the WINGX software package.[25] CCDC-242455 contains the supplementary crystallographic data for compound **1**. These data can be obtained free of charge at www.ccdc.cam.ac.uk/conts/retrieving.html (or from the Cambridge Crystallographic Data Centre, 12 Union Road, Cambridge CB2 1EZ, UK; fax: (+44) 1223-336-033; e-mail: deposit@ccdc.cam.ac.uk).

For compound **2** the powder X-ray diffraction pattern was collected on a Philips-1470 diffractometer using $Cu_{K\alpha 1}$ radiation ($\lambda = 1.54059$ Å). Data were collected by scanning in the 2θ range 5–50° with increments of 0.02°. The pattern matching was performed by using the FULLPROF program.[26]

Computational details: All the quantum calculations have been carried out by using the Gaussian03 program,[27] except the initial optimization of the trimer geometry, which was done using PC GAMESS version 6.4[28] of the GAMESS (US) package.[29] Both programs were run on computers with GNU/Linux operating systems.

Density functional theory and specifically Becke's hybrid method with three parameters[30] based on nonlocal exchange and correlation functionals, as implemented in Gaussian03 (B3LYP), has been used in all calculations. Experimental data were used as the starting point in the global optimizations of $[SiW_{12}O_{40}]^{4-}$ (T_d) and $[SiW_{11}O_{39}Cu(H_2O)]^{6-}$ (C_s, $S = {}^1/_2$) Keggin polyanions, and $[Cu_2(ac)_2(phen)_2(H_2O)_2]^{2+}$ (C_2, $S = {}^1/_2$) and $[Cu_3(ac)_3(phen)_3(H_2O)_3]^{3+}$ (C_1, $S = {}^3/_2$) cationic complexes. For the cationic complexes, the standard 6–31G(d)[31] basis has been chosen for all atoms. This basis contains polarization[32] functions in all atoms, except hydrogen. In the case of the Keggin anions, the Los Alamos effective core potential combined with a DZ basis (LANL2DZ)[33] was chosen for the transition metals, as a compromise between accuracy and computational power available, and for the remaining atoms the D95V basis[34] was used.

The exchange coupling constants J_{ij} (defined through the phenomenological Heisenberg Hamiltonian: $H_{ij} = -J_{ij} \cdot S_i \cdot S_j$) of the binuclear and trinuclear complexes have been calculated by using the broken-symmetry computational strategy of Ruiz et al.,[35] which has been shown to provide good results compared to experimental data. These calculations have used the experimental structure, since the calculated coupling constants are very sensitive to small deviations in the geometrical parameters. For the evaluation of the coupling constants of the copper(II) dimer complexes, two separate DFT calculations have been carried out, from which the energies of the triplet state (E_{HS}) and a broken-symmetry singlet configuration (E_{BS}) are obtained, whereupon the coupling constant is given approximately by Equation (7).

$$J_D = E_{BS} - E_{HS} \qquad (7)$$

To calculate both exchange coupling constants of the trinuclear complex, J_{T1} and $J_{T2,}$ the above mentioned method was carried out on a model molecule in which the copper atom not involved in the coupling is substituted by a diamagnetic Zn^{2+} ion.[36]

Besides the 6–31G(d) basis set, several combinations of the double- and triple-ζ basis sets, with or without polarization functions, of Ahlrichs and co-workers[37] were used to check its influence on the calculated values.

The magnetic molecular orbitals shown in Figure 9 were calculated with the complexes at their experimental geometries and highest spin states.

Acknowledgement

This work was supported by Universidad del País Vasco (9/UPV 00169.310–15329/2003) and Ministerio de Ciencia y Tecnología (MAT2002–03166). S.R. thanks Gobierno Vasco for his Doctoral Fellowship.

[1] a) *Polyoxometalate Chemistry for Nanocomposite Design* (Eds.: M. T. Pope, T. Yamase), Kluwer, Dordrecht, **2002**; b) *Polyoxometalates: From Topology via Self-Assembly to Applications* (Eds.: M. T. Pope, A. Müller), Kluwer, Dordrecht, **2001**; c) *Polyoxometalates: From Platonic Solids to Antiretroviral Activity* (Eds.: M. T. Pope, A. Müller), Kluwer, Dordrecht, **1994**; d) M. T. Pope, A. Müller, *Angew. Chem.* **1991**, *103*, 56; *Angew. Chem. Int. Ed. Engl.* **1991**, *30*, 34.

[2] a) C. L. Hill, *Chem. Rev.* **1998**, *98(1)*, special monographic number; b) R. Neumann, *Prog. Inorg. Chem.* **1998**, *47*, 317; c) E. Papaconstantinou, *Trends Photochem. Photobiol.* **1994**, *3*, 139; d) N. Fukuda T. Yamase, Y. Tajima, *Biol. Pharm. Bull.* **1999**, *22*, 463; e) C. L. Hill, M. S. Weeks, R. F. Schinazi, *J. Med. Chem.* **1990**, *33*, 2767; f) A. Müller, C. Serain, *Acc. Chem. Res.* **2000**, *33*, 2; g) J. M. Clemente-Juan, E. Coronado, *Coord. Chem. Rev.* **1999**, *193–195*, 361; h) M. Clemente-León, E. Coronado, P. Delhaes, C. J. Gómez-García, C. Mingolaud, *Adv. Mater.* **2001**, *13*, 574; i) L. Ouahab, *Coord. Chem. Rev.* **1998**, *178–180*, 1501.

[3] For recent works see: a) G. Li, Z. Shi, Y. Xu, S. Feng, *Inorg. Chem.* **2003**, *42*, 1170; b) R. C. Finn, J. Sims, C. J. O'Connor, J. Zubieta, *J. Chem. Soc. Dalton Trans.* **2002**, *159*; c) R. L. Laduca, Jr., R. S. Rarig, Jr., J. Zubieta, *Inorg. Chem.* **2001**, *40*, 607; d) J. Do, A. J. Jacobson, *Inorg. Chem.* **2001**, *40*, 2468; e) P. J. Hagrman, J. Zubieta, *Inorg. Chem.* **2001**, *40*, 2800.

[4] For recent works see: a) C.-Z. Lu, C.-D. Wu, H.-H. Zhuang, J.-S. Huang, *Chem. Mater.* **2002**, *14*, 2649; b) R. S. Rarig, Jr., J. Zubieta, *J. Solid State Chem.* **2002**, *167*, 370; c) W. Yang, C. Lu, H. Zhuang, *J. Chem. Soc. Dalton Trans.* **2002**, 2879; d) C.-D. Wu, C.-Z. Lu, H.-H. Zhuang, J.-S. Huang, *Inorg. Chem.* **2002**, *41*, 5636; e) P. J. Hagrman, J. Zubieta, *Inorg. Chem.* **2000**, *39*, 5218.

[5] a) P. Mialane, A. Dolbecq, E. Rivière, J. Marrot, F. Sécheresse, *Eur. J. Inorg. Chem.* **2004**, 33; b) A. Dolbecq, P. Mialane, L. Lisnard, J. Marrot, F. Sécheresse, *Chem. Eur. J.* **2003**, *9*, 2914; c) G. Luan, Y. Li, S. Wang, E. Wang, Z. Hang, C. Hu, N. Hu, H. Jia, *Dalton Trans.* **2003**, 233; d) J.-Y. Niu, M.-L. Wei, J.-P. Wang, D.-B. Dang, *J. Mol. Struct.* **2003**, *655*, 171; e) R. Nandini Devi, E. Burkholder, J. Zubieta, *Inorg. Chim. Acta* **2003**, *348*, 150; f) S. Uchida, M. Hashimoto, N. Mizuno, *Angew. Chem.* **2002**, *114*, 2938; *Angew. Chem. Int. Ed.* **2002**, *41*, 2814; g) Y. Xu, J.-Q. Xu, K.-L. Zhang, Y. Zhang, X.-Z. You, *Chem. Commun.* **2000**, 153.

[6] S. Reinoso, P. Vitoria, L. Lezama, A. Luque, J. M. Gutiérrez-Zorrilla, *Inorg. Chem.* **2003**, *42*, 3709.

[7] a) Formula: $C_{70}H_{103}Cu_7N_{10}O_{112}Rb_7Si_2W_{22}$, $M_w = 8020.6\ g\,mol^{-1}$; crystal system: triclinic; space group: $P\bar{1}$, $a = 17.94(1)$, $b = 17.98(2)$, $c = 23.89(2)$ Å, $\alpha = 87.87(7)$, $\beta = 88.42(6)$, $\gamma = 85.42(7)°$, $V = 7672$ Å^3; b) $a = 18.040(4)$, $b = 18.075(4)$, $c = 24.088(4)$ Å, $\alpha = 87.88(3)$, $\beta = 88.64(2)$, $\gamma = 84.71(1)°$, $V = 7814(3)$ Å^3, $\rho_{calcd} = 3.409(6)\ g\,cm^{-3}$; diffractometer: Philips-1470, θ limits: 5.1–50°; refined parameters: 9; $Rp = 3.46$; $\chi^2 = 3.76$.

[8] U. Kortz, S. Matta, *Inorg. Chem.* **2001**, *40*, 815.

[9] J. R. Galán-Mascarós, C. Giménez-Saiz, S. Triki, C. J. Gómez-García, E. Coronado, L. Ouahab, *Angew. Chem.* **1995**, *107*, 1601; *Angew. Chem. Int. Ed. Engl.* **1995**, *34*, 1460.
[10] a) H. T. Evans, Jr., T. J. R. Weakley, G. B. Jameson, *J. Chem. Soc. Dalton Trans.* **1996**, 2537; b) B. Yan, Y. Xu, X. Bu, N. K. Goh, L. S. Chia, G. D. Stucky, *J. Chem. Soc. Dalton Trans.* **2001**, 2009.
[11] a) L. Lisnard, A. Dolbecq, P. Mialane, J. Marrot, F. Sécheresse, *Inorg. Chim. Acta* **2004**, *357*, 845; b) L. San Felices, P. Vitoria, J. M. Gutiérrez-Zorrilla, S. Reinoso, J. Etxeberria, L. Lezama, *Chem. Eur. J.* **2004**, *10*, 5138.
[12] T. Tokii, N. Watanabe, M. Nakashima, Y. Muto, M. Morooka, S. Ohba, Y. Saito, *Bull. Chem. Soc. Jpn.* **1990**, *63*, 364.
[13] D. K. Towle, S. K. Hoffman, W. E. Hatfield, P. Singh, P. Chaudhuri, *Inorg. Chem.* **1988**, *27*, 394.
[14] E. Wasserman, L. C. Snyder, W. A. Yager, *J. Chem. Phys.* **1964**, *41*, 1763.
[15] A. Bencini, D. Gatteschi, *Electron Paramagnetic Resonance of Exchange Coupled Systems*, Springer, Berlin, **1990**.
[16] O. Kahn, *Molecular Magnetism*, VCH, New York, **1993**.
[17] B. Bleaney, K. D. Bowers, *Proc. R. Soc. London, Proc. R. Soc. London Ser. A* **1952**, *214*, 451.
[18] R. L. Carlin, *Magnetochemistry*, Spinger, Berlin, **1986**.
[19] A. Rodríguez-Fortea, P. Alemany, S. Alvarez, E. Ruiz, *Chem. Eur. J.* **2001**, *7*, 627.
[20] A. Tézé, G. Hervé, *J. Inorg. Nucl. Chem.* **1977**, *39*, 999
[21] Oxford Diffraction, CrysAlis CCD and RED. Version 1.70, Oxford Diffraction Ltd., Oxford (UK), **2003**.
[22] *International Tables for X-ray Crystallography*; *Vol. IV*, Kynoch Press, Birmingham, **1974**.
[23] P. T. Beurkens, G. Beurkens, R. de Gelder, S. García-Granda, R. O. Gould, R. Israel, J. M. M. Smits, The DIRDIF Program System. Technical Report of the Crystallography Laboratory, University of Nijmegen, Nijmegen (The Netherlands), **1999**.
[24] G. M. Sheldrick, SHELXL97, Program for crystal structure refinement, University of Göttingen, Göttingen (Germany), **1997**.
[25] L. J. Farrugia, WINGX, a Windows Program for Crystal Structure Analysis, University of Glasgow, Glasgow (UK), **1999**.
[26] J. Rodríguez-Carvajal, *Physica* **1992**, *192*, 55.
[27] M. J. Frisch, G. W. Trucks, H. B. Schlegel, G. E. Scuseria, M. A. Robb, J. R. Cheeseman, J. A. Montgomery, Jr., T. Vreven, K. N. Kudin, J. C. Burant, J. M. Millam, S. S. Iyengar, J. Tomasi, V. Barone, B. Mennucci, M. Cossi, G. Scalmani, N. Rega, G. A. Petersson, H. Nakatsuji, M. Hada, M. Ehara, K. Toyota, R. Fukuda, J. Hasegawa, M. Ishida, T. Nakajima, Y. Honda, O. Kitao, H. Nakai, M. Klene, X. Li, J. E. Knox, H. P. Hratchian, J. B. Cross, C. Adamo, J. Jaramillo, R. Gomperts, R. E. Stratmann, O. Yazyev, A. J. Austin, R. Cammi, C. Pomelli, J. W. Ochterski, P. Y. Ayala, K. Morokuma, G. A. Voth, P. Salvador, J. J. Dannenberg, V. G. Zakrzewski, S. Dapprich, A. D. Daniels, M. C. Strain, O. Farkas, D. K. Malick, A. D. Rabuck, K. Raghavachari, J. B. Foresman, J. V. Ortiz, Q. Cui, A. G. Baboul, S. Clifford, J. Cioslowski, B. B. Stefanov, G. Liu, A. Liashenko, P. Piskorz, I. Komaromi, R. L. Martin, D. J. Fox, T. Keith, M. A. Al-Laham, C. Y. Peng, A. Nanayakkara, M. Challacombe, P. M. W. Gill, B. Johnson, W. Chen, M. W. Wong, C. González, J. A. Pople, Gaussian03, Revision B.05, Gaussian, Inc., Pittsburgh PA (USA), **2003**.
[28] A. A. Granovsky, http://classic.chem.msu.su/gran/gamess/index.html.
[29] M. W. Schmidt, K. K. Baldridge, J. A. Boatz, S. T. Elbert, M. S. Gordon, J. J. Jensen, S. Koseki, N. Matsunaga, K. A. Nguyen, S. Su, T. L. Windus, M. Dupuis, J. A. Montgomery, *J. Comput. Chem.* **1993**, *14*, 1347.
[30] A. D. Becke, *J. Chem. Phys.* **1993**, *98*, 5648.
[31] a) A. J. H. Wachters, *J. Chem. Phys.* **1970**, *52*, 1033; b) P. J. Hay, *J. Chem. Phys.* **1977**, *66*, 4377; c) K. Raghavachari, G. W. Trucks, *J. Chem. Phys.* **1989**, *91*, 1062.
[32] M. J. Frisch, J. A. Pople, J. S. Winkley, *J. Chem. Phys.* **1984**, *80*, 3265.
[33] a) P. J. Hay, W. R. Wadt, *J. Chem. Phys.* **1985**, *82*, 270; b) W. R. Wadt, P. J. Hay, *J. Chem. Phys.* **1985**, *82*, 284; c) P. J. Hay, W. R. Wadt, *J. Chem. Phys.* **1985**, *82*, 299.
[34] T. H. Dunning, Jr., P. J. Hay in *Modern Theoretical Chemistry*, *Vol. 3* (Ed.: H. F. Schaefer III), Plenum, New York, **1976**, pp. 1–28.
[35] E. Ruiz, P. Alemany, S. Alvarez, J. Cano, *J. Am. Chem. Soc.* **1997**, *119*, 1297.
[36] E. Ruiz, J. Cano, S. Alvarez, A. Caneschi, D. Gatteschi, *J. Am. Chem. Soc.* **2003**, *125*, 6791.
[37] a) A. Schaefer, H. Horn, R. Ahlrichs, *J. Chem. Phys.* **1992**, *97*, 2571; b) A. Schaefer, C. Huber, R. Ahlrichs, *J. Chem. Phys.* **1994**, *100*, 5829.

Received: July 23, 2004
Published online: January 20, 2005